JOURNAL OF FORENSIC SCIENCES

J Forensic Sci, September 2011, Vol. 56, No. 5
doi: 10.1111/j.1556-4029.2011.01835.x
Available online at: onlinelibrary.wiley.com

PAPER

CRIMINALISTICS

Nima Behrooz,[1] *B.Sc.; Lee Hulse-Smith,*[2] *M.S.; and Sanjeev Chandra,*[1] *Ph.D.*

An Evaluation of the Underlying Mechanisms of Bloodstain Pattern Analysis Error

ABSTRACT: An experiment was designed to explore the underlying mechanisms of blood disintegration and its subsequent effect on area of origin (AO) calculations. Blood spatter patterns were created through the controlled application of pressurized air (20–80 kPa) for 0.1 msec onto suspended blood droplets (2.7–3.2 mm diameter). The resulting disintegration process was captured using high-speed photography. Straight-line triangulation resulted in a 50% height overestimation, whereas using the lowest calculated height for each spatter pattern reduced this error to 8%. Incorporation of projectile motion resulted in a 28% height underestimation. The AO *xy*-coordinate was found to be very accurate with a maximum offset of only 4 mm, while AO size calculations were found to be two- to fivefold greater than expected. Subsequently, reverse triangulation analysis revealed the rotational offset for 26% of stains could not be attributed to measurement error, suggesting that some portion of error is inherent in the disintegration process.

KEYWORDS: forensic science, bloodstain pattern analysis, fluid dynamics, blood

Measurements taken from bloodstain spatter patterns at a crime scene can be utilized to calculate the associated bloodshed area of origin (AO) within a three-dimensional space. Generally, this involves the resolution of individual spatter patterns, selection of suitable bloodstains within, resolution of impact direction, stain triangulation to yield a two-dimensional area of convergence, and finally overlaying this with the third dimension, height, by calculating bloodstain impact angles via the Balthazard formula (1). Once determined, the AO can prove useful in reconstructing the events surrounding bloodshed. Research examining the accuracy and underlying mechanisms of this methodology is still incomplete.

Within the bloodstain pattern analysis (BPA) community, variation exists in methodologies used for pattern recognition, velocity categorization, stain selection, and stain measurement. Despite this variation, there is a strong scientific foundation for correlations between certain stain morphology parameters and the AO. These include impact directionality through the presence of one or more spines, triangulation using the long axis (l) of multiple stain ellipses, and the angle of impact using the ratio of the long axis (l) to short axis (w) through application of the Balthazard formula (Eq. [1]). By combining all three parameters, the final AO can be established within a three-dimensional space (2).

$$\sin\theta = \frac{w}{l} \tag{1}$$

As projectile motion has proven difficult to incorporate into AO modeling, straight-line flight paths are assumed with the inherent limitation that the z-coordinate will be consistently overestimated. In response, the BPA community recommends presenting the AO z-coordinate as a maximum height calculation (3).

With a few exceptions (1,4), research into BPA error rates typically utilize a mock crime scene approach, or focus on individual passive droplets (5–11). Researchers employing a mock crime scene approach are usually attempting to replicate the conditions of a specific criminal case. This can only provide a rough estimate of AO error, because the experiments are highly variable and difficult to control. To establish greater control, researchers have turned to the study of passive droplets, which usually involves individual blood droplets of a standard size made to fall under the influence of gravity alone. However, this approach is limited to investigating the error associated with the AO z-coordinate component, because triangulation of multiple stains within a spatter pattern is required to evaluate the AO size and xy-coordinate.

This currently limits any complete evaluation of the AO to the mock crime scene approach. The consequence of which makes it very difficult to explore the underlying mechanisms related to error. Take for example a typical experiment where some force (hand, baseball bat, firearm projectile) is applied to some blood source (blood-soaked sponge, pool of blood). Subsequently, AO is triangulated from the resulting spatter pattern and compared with the known AO. With the exception of z-coordinate overestimation resulting from straight-line triangulation, it would be tempting to conclude that any observed error must be related to the analyst's measurement technique. This overlooks an important variable, highlighted in Fig. 1. Each frame represents a 10-msec interval following the impact of a hammer on a pool of blood. This series of high-speed photographs represents one in a series of disintegration events captured by Taylor et al., available online (http://www.ameslab.gov/mfrc/rd) (12). It is clear from these images that a number of complex fluid dynamic events are present. Therefore, it seems reasonable to speculate that some degree of AO error might be related to blood displacement and disintegration from an often complicated and variable collision.

[1]Departmental of Mechanical and Industrial Engineering, University of Toronto, 5 King's College Road, Toronto, Ontario M5S 3G8, Canada.
[2]Centre of Forensic Sciences, 25 Grosvenor Street, Toronto, Ontario M7A 2G8, Canada.

Received 18 May 2010; and in revised form 2 Sept. 2010; accepted 11 Sept. 2010.

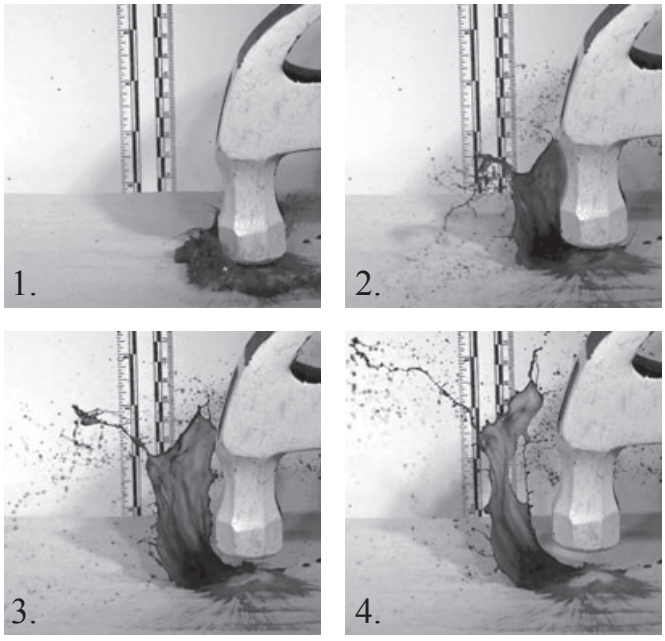

FIG. 1—*High-speed photographs of a hammer impacting a pool of blood. Images are numbered according to increasing time intervals of 10 msec (http://www.ameslab.gov/mfrc/rd) (12).*

Research into the dynamics of fluids other than blood offers some insight into this complex interaction (13–15). It begins when an object strikes a liquid source, transferring energy through compression and forcing liquid displacement away from the strike point. The amount of transferred energy will correlate with the degree of fluid displacement. As the liquid undergoes displacement, the ratio of surface area to volume increases. To counter this instability, the displaced liquid will either recoil through counteracting surface tension forces or disintegrate into smaller fragments where the energy is great enough. Ultimately, aerodynamic forces govern droplet size. The higher the velocity of blood displacement, the greater the instability created at the liquid–gas interface, resulting in the generation of smaller droplets. This provides some support for the current correlations made within the BPA community between bloodstain size and droplet velocity. Liquid displacement is quite complex, however, and not all of the liquid will be traveling at the same velocity. This could result in a variety of droplet sizes, in addition to the generation of sheets and filaments. As blood has a relatively high viscosity when compared to water, this increased resistance to flow will counteract displacement and increase the probability of encountering sheets and filaments, as readily observed in Fig. 1. Unlike droplets, sheets and filaments are inherently unstable because of their higher surface area-to-volume ratio and will either recoil into a single droplet or further disintegrate into multiple droplets.

Once airborne, droplet flight trajectory is governed by the effects of gravity and drag (or air resistance). Gravity results in downward droplet acceleration and can be modeled using the following projectile motion equations:

$$y(t) = -\frac{1}{2}gt^2 + v_{oy}t + y_o \tag{2}$$

$$v_y(t) = -gt + v_{oy} \tag{3}$$

$$a_y(t) = -g \tag{4}$$

$$v_x(t) = v_{ox} = v_o \cos\theta_o \tag{5}$$

$$x(t) = v_{xo}t + x_o \tag{6}$$

$$a_x(t) = 0 \tag{7}$$

$$\tan\theta = \frac{v_y}{v_x} \tag{8}$$

The force applied to the body of a droplet in motion by the surrounding air is called drag and acts in the opposite direction of droplet motion. The value of drag force can be calculated using the following equation:

$$F_{\text{Drag}} = C_D\left[\frac{1}{2}\rho_{\text{air}}V^2\left(\frac{\pi}{4}D^2\right)\right] \tag{9}$$

where ρ is the fluid density, V is the flow velocity, and D is the droplet diameter. C_D is the coefficient of drag, which is a function of Reynolds number and depends on the shape of the object. The Reynolds number for a sphere is defined as:

$$\text{Re} = \frac{\rho D_o V_o}{\mu} \tag{10}$$

where D is the droplet diameter, and μ is the fluid viscosity.

The aim of this research was to utilize a novel experimental design to investigate the error associated with the standard calculations for AO. Starting with a mock crime scene experimental approach, the initial volume of blood was significantly reduced, and the disintegration process was propagated through the application of a short burst of pressurized air. These two modifications allowed for better resolution of the disintegration process to provide a window into the underlying mechanisms responsible for AO error.

Materials and Methods

A gas tank filled with pressurized air was connected to a nozzle via stainless steel tubing. A pressure gauge was used to measure air pressure, while a solenoid valve with digital pulse generator ensured a controlled release of air from the nozzle. This apparatus was contained within an aluminum frame structure to allow for vertical adjustment. Iron plates secured to the structure ensured it would not move during operation. A diagram of this experimental setup is shown in Fig. 2.

A syringe, mounted within a syringe pump to regulate flow rate, was connected to a stainless steel needle using clear plastic tubing. The syringe and needle were clamped within the apparatus such that a droplet suspended from the needle would be directly within the path of pressurized air released from the nozzle. Pig blood was chosen owing to similarities in physical properties with human blood. The reader is directed to our previous article for additional information regarding these properties (10).

Fresh pig blood was obtained from an abattoir (Quality Meat Packers, Toronto, Ontario, Canada) and stored in test tubes containing the anticoagulant ethylenediaminetetraacetic acid (EDTA). The blood was stored at 4°C and was used within 48 h of collection. Blood was placed into the syringe pump, which was then utilized to deliver a specific volume of blood, resulting in consistent sized blood droplets suspended from the needle tip. Droplet diameter was measured directly from the high-speed images taken immediately prior to disintegration, using the needle diameter as a calibration reference. Blood droplet and needle diameters are shown in Table 1. While these are the same needles used in our previous

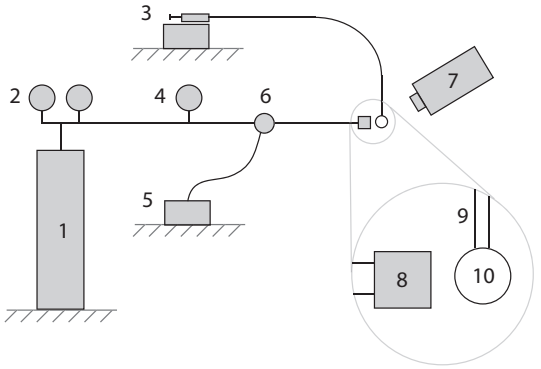

FIG. 2—*Experimental setup: (1) Compressed air cylinder, (2) Pressure regulators, (3) Syringe and syringe pump, (4) Pressure gauge, (5) Pulse generator, (6) Solenoid valve, (7) High-speed camera, (8) Nozzle, (9) Needle, (10) Blood droplet.*

TABLE 1—*Droplet diameter was measured from high-speed photographs taken 0.5 msec prior to droplet disintegration. Image calibration was performed using the needle outer diameter.*

Syringe Needle			
Gauge	Inner Diameter (mm)	Outer Diameter (mm)	Droplet Diameter (mm)
12	2.8	2.2	3.2 ± 0.11 (n = 4)
17	1.5	1.1	2.7 ± 0.13 (n = 6)

research (10), the droplet diameters generated here have been reduced to prevent droplet detachment under gravity prior to the application of pressurized air.

The pulse generator was set to allow air release from the nozzle for 0.1 msec. This resulted in complete separation of the blood droplet from the needle and subsequent disintegration into smaller droplets. A FastCam-Ultima 1024 high-speed video camera (Photron, Tokyo, Japan) was used to capture the disintegration of droplets from the syringe needle at 1000 frames per second. The camera was positioned 0.5 m from the droplet such that it could capture disintegration from a side view. A light source was placed 1.5 m from the droplet on the opposite side to optimize image contrast. The camera was connected to the pulse generator to synchronize image capture with air release from the nozzle.

The initial velocity of projected droplets was obtained by measuring the distance traveled by individual droplets between each frame of the high-speed camera images. The known needle diameter was used for calibration. The resulting blood spatter pattern was captured on standard white printing paper positioned 86 mm below the nozzle. The AO *xy*-coordinate was marked on the paper prior to each experimental run by releasing a single droplet from the needle and allowing it to impact on the paper. Bloodstains were allowed to dry prior to digital conversion via a high-resolution scanner. All digital measurements were conducted using either the ImageJ (U.S. National Institute of Health, Bethesda, MD) or Adobe Illustrator (Adobe, San Jose, CA) imaging software.

The experiment was conducted using two different needle sizes (to vary droplet diameter) and four different air pressures (to vary impact velocity). Each experiment was replicated three times, resulting in the generation of 24 blood spatter patterns. Where applicable, data comparison was undertaken using Neyman–Pearson statistical testing with a 95% confidence interval.

Results and Discussion

Figures 3 and 4 show a side-by-side comparison of two blood droplets undergoing disintegration. The two columns represent different applied air pressures (20 and 40 kPa). Droplet diameter was kept constant at 3.2 mm. The images show the process of disintegration over 25 msec following the application of pressurized air onto the droplet for 0.1 msec.

At time zero, the droplets can be seen adhering to the needle tip, representing the known AO. At 3 msec, the pressurized air has already been applied and sheets, filaments, and individual droplets can be seen radiating from the AO. At 5 msec, small droplets *c.* 0.5 mm in diameter are moving away from the AO at *c.* 6 m/sec. These are byproducts of the initial pressurized air flowing over the liquid surface, causing sufficient instability to produce droplets of this size.

At 10 msec, the 40 kPa air pressure is associated with the generation of more droplets than the 20 kPa air pressure. At both pressures, a substantial volume of blood can still be observed close to the AO. By 20 msec, this volume of blood has begun to stabilize into droplets *c.* 1–1.5 mm in diameter traveling away from the AO at a relatively low velocity of *c.* 1 m/sec. By 25 msec, only larger droplets and a few filaments remain.

The resulting 24 spatter patterns exhibited similar characteristics. Figure 5 represents a 0.2 × 0.2 m portion of one spatter pattern. Each spatter pattern was comprised of *c.* 200 stains covering an area of about 1.1 × 0.2 m. Of these stains, about 75% were

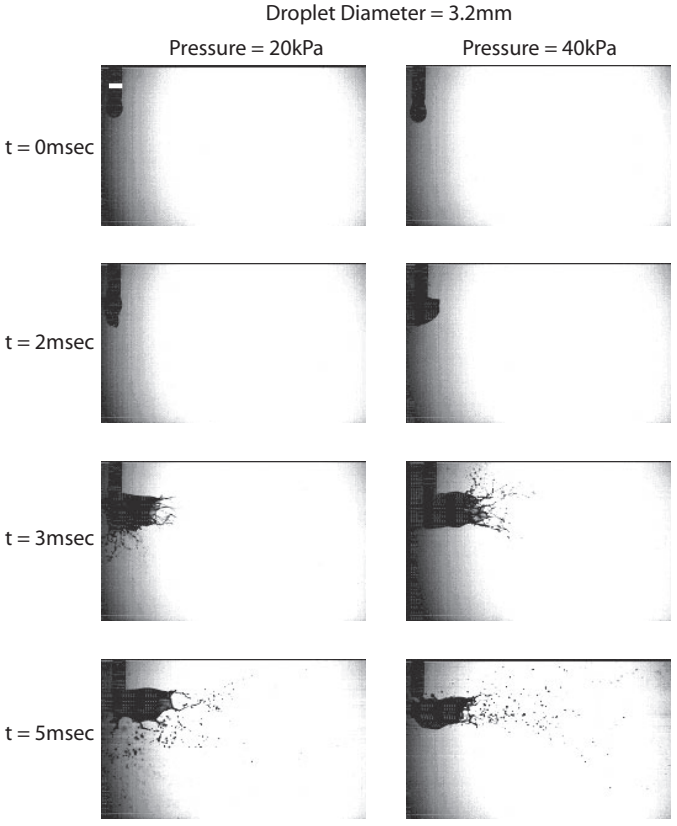

FIG. 3—*High-speed photograph time-series comparing the blood droplet disintegration process following application of 20 and 40 kPa pressurized air for 0.1 msec. Droplet diameter was kept constant at 3.2 mm. Needle diameter, which is marked with a white calibration line in the top left image, is 2.8 mm. This time-series continues in Fig. 4.*

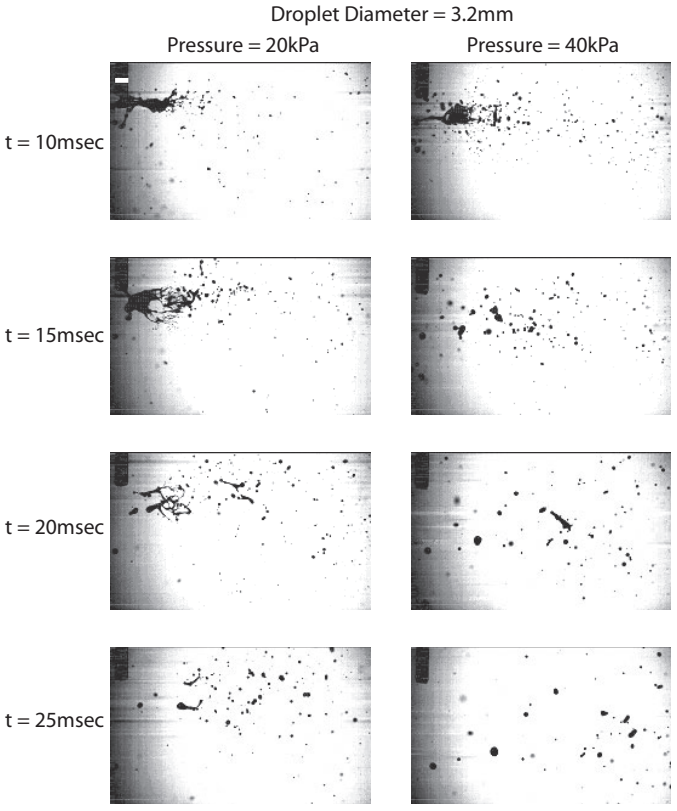

FIG. 4—*High-speed photograph time-series continued from Fig. 3.*

FIG. 5—*A 0.2 × 0.2 m section of one blood spatter. The area of origin is located 0.31 m from the bottom edge of this section. Applied air pressure was 80 kPa and droplet diameter was 3.2 mm.*

<0.5 mm diameter with no indication of directionality. This left between 30 and 60 stains per spatter pattern, which could yield directionality, with elliptical short axis ranging between 0.5 and 6 mm. Stain selection and measurements were based on the criteria outlined by Wells (16). These included:

- Well-formed stains
- Angle of impact <60°
- Equal number of stains from each side of the spatter pattern
- Within 50% of distance from the furthest stain
- Approximately 20 stains

Unfortunately for each spatter pattern, after applying the first four criteria listed above, only 8–12 stains were deemed suitable. The *z*-coordinate (height) was calculated using the Balthazard formula based on the long and short axis of a best-fit ellipse overlayed within the ImageJ software, as demonstrated in Fig. 6. Care was taken when fitting each ellipse to account for the asymmetrical nature of each bloodstain (16). The long axis was subsequently extracted from each ellipse and then scaled to provide triangulation lines back to the AO. For the purposes of triangulation, this method prevented any measurement bias as the long axis was determined while zoomed into the digital image for each stain, thereby hiding the known AO.

Figure 7 highlights the error associated with the *z*-coordinate for each starting blood droplet diameter and applied air pressure. With a known *z*-coordinate of 86 mm, these results show an average overestimation of 43 mm (50% error), with a range of 16–64 mm. No statistically significant relationship was found between the degree of *z*-coordinate offset and either air pressure or droplet size. These overestimations were expected given that straight-line triangulation does not account for projectile motion and drag. As a result, two alternative methods for estimating the *z*-coordinate were explored. The first examines the accuracy of reporting the lowest *z*-coordinate as a best estimate calculation. The second explores whether projectile motion and drag could be incorporated into AO modeling.

As straight-line triangulation consistently overestimates the *z*-coordinate, the lowest *z*-coordinate measurement for each spatter pattern was considered as a potential alternative. The results of this approach are shown in Fig. 8. The average overestimation was reduced from 43 to 7 mm (8% error) with a range between −10 and 29 mm. In a few cases, the lowest *z*-coordinate resulted in an underestimation. As using straight lines to estimate *z*-coordinate should always result in an overestimation, we attribute this to measurement error. As a result, if this method is utilized in casework, it should be reported as a best estimate and not as a maximum height calculation. It should also be noted that it will be impossible to determine the variation around this best estimate because this approach only utilizes a single point.

Next, projectile motion and drag were explored to determine whether they might be utilized to reduce *z*-coordinate error. The following projectile motion equations were derived.

FIG. 6—*A bloodstain shown on the right with its best-fit ellipse on the left.*

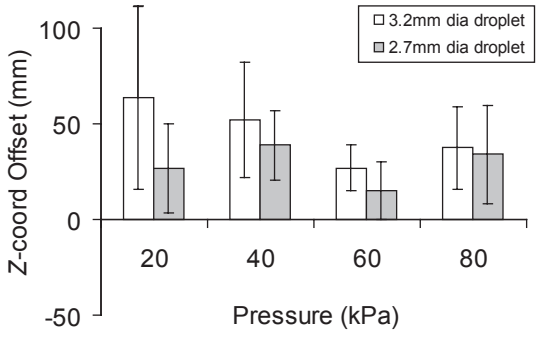

FIG. 7—*The average* z*-coordinate offset over four applied air pressures and two droplet diameters. Error bars represent the 95% confidence interval.*

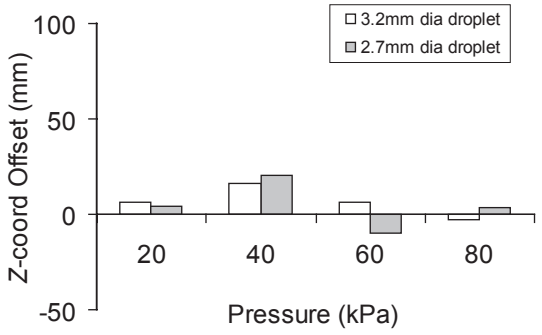

FIG. 8—*The lowest* z*-coordinate offset over four applied air pressures and two droplet diameters.*

From Eqs (3), (5), and (8), the time of flight can be solved

$$\tan\theta = \frac{-gt}{v_o \cos\theta_o}$$

or

$$t = \frac{\tan\theta v_o \cos\theta_o}{-g} \tag{11}$$

then substitute Eq. (11) into Eq. (5) to solve for initial velocity

$$x(t) = \frac{\tan\theta \cos^2\theta_o v_o^2}{-g}$$

or

$$v_o = \sqrt{\frac{-x(t)g}{\tan\theta \cos^2\theta_o}} \tag{12}$$

and finally substitute Eq. (11) into Eq. (2) where $y(t) = 0$ to solve for height

$$y_o = -\left(\frac{\tan\theta v_o \cos\theta_o}{-g}\right)\left(\frac{\tan\theta v_o \cos\theta_o}{2} + v_{oy}\right) \tag{13}$$

From Eqs (12) and (13), the initial droplet velocity (v_o) and z-coordinate (y) can be derived from the droplet launch angle (θ_o), horizontal distance (x), and impact angle (θ). The launch angle is currently not attainable from spatter pattern measurements, presenting a significant limitation to utilizing this approach in casework.

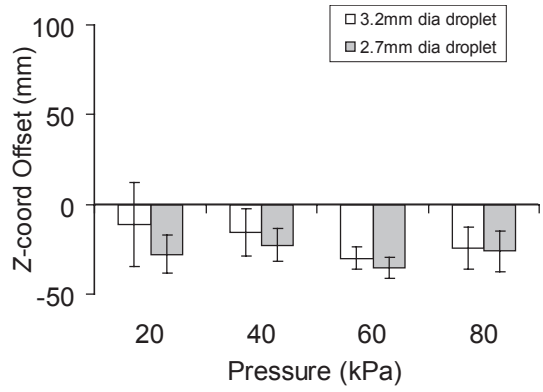

FIG. 9—*Projectile motion equations were used to predict the* z*-coordinate over the four applied air pressures and two droplet diameters tested. Error bars represent the 95% confidence interval.*

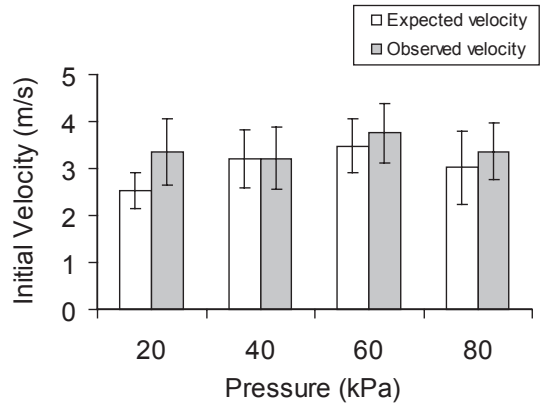

FIG. 10—*Projectile motion equations were used to predict the initial velocity over the four applied air pressures and two droplet diameters tested. Observed initial velocity was derived from high-speed photographs of droplet disintegration. Error bars represent the 95% confidence interval.*

For the purposes of analysis, however, the known horizontal launch angle of 0° was used. Figures 9 and 10 show these results for predicting the z-coordinate and initial velocity, respectively.

On average, projectile motion calculations result in a z-coordinate underestimation of −24 mm (28% error) with a range between −11 and −35 mm. The initial velocity values derived from projectile motion equations do not differ statistically from the velocity values measured from the high-speed photographs of droplet disintegration. This underestimation could result from assuming a 0° launch angle. From the high-speed photographs, it is clear that blood droplets are projected over a variety of angles. Also, the exclusion of drag forces could be a factor. However, if this were the case, a similar underestimation of velocity would have been expected.

Drag is proportional to the square of droplet velocity and inversely proportional to a droplets diameter. Consequently, small fast droplets are more susceptible to these effects. To study the consequence of ignoring drag, blood droplet deceleration was modeled using Eq. (9) for droplet diameters and velocities observed in this experiment. These calculations are shown in Fig. 11. These error calculations demonstrate that drag forces must be taken into account for all droplets with initial velocities >3 m/sec. Otherwise, for droplet >1.6 mm diameter and traveling <3 m/sec, the effects of drag can generally be ignored with minimal impact on z-coordinate

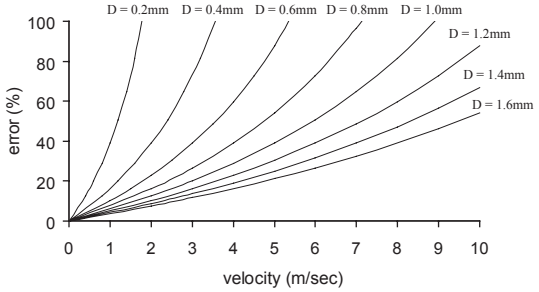

FIG. 11—*Effect of drag forces on blood droplets between 0.2 and 1.6 mm in diameter, traveling up to 10 m/sec. Drag coefficient was set to 1.*

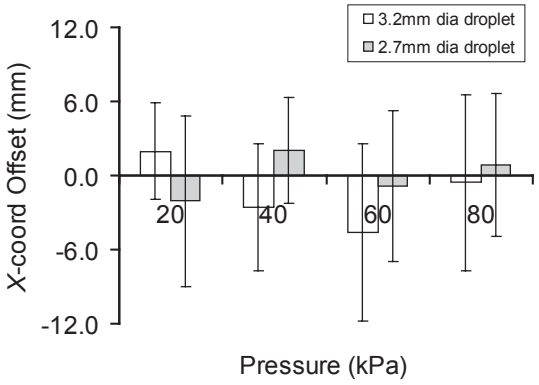

FIG. 12—XY-*coordinate offset was calculated for each of four air pressures and two droplet diameters tested. Offset was calculated for each triangulation line at the point which it crossed the known* x-*axis (*y-*coordinate = 0). Error bars represent the 95% confidence interval and were used to assess the area of origin size.*

calculations. In this experiment, the stain selection criteria favored larger stains. With this in mind, the larger droplets within the high-speed images were found to be >0.8 mm diameter and traveling <3 m/sec. Therefore, ignoring drag is expected to introduce no more than 30% error in predicting the *z*-coordinate in this experiment. This is quite substantial and highlights that any attempt to incorporate projectile motion into AO modeling must take drag into account.

AO error associated with size and *xy*-coordinate was calculated using the stain triangulation lines at the point with which they crossed the known *x*-axis, which runs perpendicular to the spatter flight direction. For each spatter pattern, the *xy*-coordinate was measured as the average offset between each triangulation line and the known *xy*-coordinate, while AO size was measured as the 95% confidence interval of this average. These calculations are presented in Fig. 12.

No statistically significant correlations were found between the observed errors, and blood volumes and velocities tested. *XY*-coordinates were found to be quite accurate, with the least accurate spatter pattern deviating from the known *xy*-coordinate by only 4 mm. On the other hand, the AO size was found to be larger than expected. The known blood droplet diameters tested were 2.7 and 3.2 mm, while the calculated sizes ranged between 7.8 and 14.3 mm, representing a two- to fivefold increase. Further analysis of these results revealed a number of outliers present within each trial. This was investigated further.

One of the 24 spatter patterns was selected randomly for additional analysis. The stain selection criteria were lowered to include

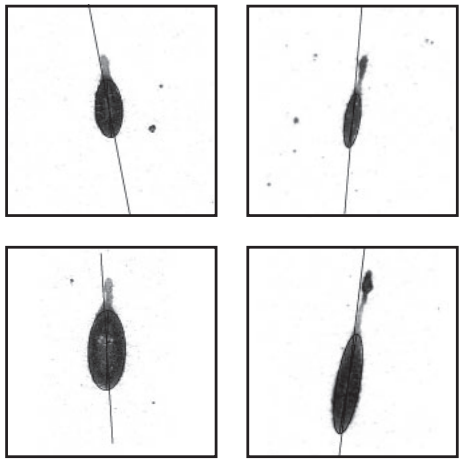

FIG. 13—*Four bloodstains from one spatter pattern are shown. Lines represent the triangulation lines starting from the known* xy-*position.*

stains that could provide a measure of directionality only. This resulted in the selection of 54 stains. For the purpose of this analysis, instead of starting at each stain and triangulating "backward," the known *xy*-position was used as the starting point and lines were drawn "forward" out to each stain. Where each line overlapped the corresponding stain, the rotational offset could then be evaluated. Of these 54 stains, the rotational offsets of 14 (26%) were significant enough that it was reasonable to assume that any individual tasked with fitting an ellipse to a bloodstain was unlikely to have arrived at the same triangulation line. Four of these representative stains are shown in Fig. 13 each with their corresponding triangulation path originating from the known *xy*-coordinate. This finding clearly demonstrates that a component of AO error is not related to analyst measurement but is instead inherent in the process of blood displacement and disintegration.

Postimpact droplet formation is the most likely mechanism for this contribution to AO size error. This "fork in the road" effect occurs when a blood volume structure (sheet, filament, or large droplet) has traveled a certain distance from the AO and reaches an instability threshold where it disintegrates into smaller volumes. Subsequently, trajectory lines for these respective bloodstains will triangulate back to this fork in the road where secondary disintegration occurred, instead of back to the true AO. Given that this experiment was designed to reduce the complexity of droplet disintegration, it is likely that this will be more predominant under bloodshed conditions more typically associated with crime scenes.

Conclusion

Small volumes of blood were disintegrated through the application of pressurized air. The resulting spatter patterns were used to evaluate BPA AO error and investigate the underlying mechanisms. Under these experimental conditions, *z*-coordinate predictions were consistently overestimated by an average of 50%, while using the lowest *z*-coordinate within a spatter pattern reduced this error to 8%. However, if this value is to be reported, it should be presented as an estimate and not as a maximum height calculation. Incorporation of projectile motion into *z*-coordinate calculations was found to underestimate by an average of 28%, while velocity predictions were found to be quite accurate when compared with the high-speed photographs. However, the application of projectile motion is limited at this time as an assumption related to launch angle was required, and the impact of drag could not be ignored.

XY-coordinate predictions were found to be accurate, with the greatest offset being only 4 mm. However, AO size estimates were found to be two- to fivefold greater than the true AO size. Additional investigation revealed that 26% of the stains within a randomly selected spatter pattern exhibited rotational offset that could not be accounted for by measurement error. A ''fork in the road'' mechanism was proposed to explain this offset, whereby unstable blood volume structures undergo secondary disintegration after first traveling some distance from the AO.

References

1. Balthazard V, Piedelievre R, Desoille H, Derobert L. Study of projected droplets of blood. Ann Med Leg Criminol Police Sci Toxicol 1939;19(4):265–323.
2. Carter AL, Podworny EJ. Bloodstain pattern analysis with a scientific calculator. Can Soc Forensic Sci J 1991;24(1):37–42.
3. James SH, Eckert WG. Interpretation of bloodstain evidence at crime scenes, 2nd edn. New York, NY: CRC Press, 1999.
4. Raymond MA, Liesegang J, Smith ER. High speed cinematography of blood droplet deformation in flight—implications for crime scene reconstruction. In: Jacob B, Bonte W, editors. Advances in forensic sciences—Proceedings of the 13th Meeting of the International Association of Forensic Sciences; 1993 Aug 22–28; Düsseldorf, Germany. Berlin, Germany: Verlag Dr. Köster, 1995;200–7.
5. Carter AL. Directional analysis of bloodstain patterns theory and directional analysis. J Forensic Identification 2006;56(2):242–56.
6. Karger B, Nusse R, Bajanowski T. Backspatter on the firearm and hand in experimental close-range gunshots to the head. Am J Forensic Med Path 2002;23(3):211–3.
7. Randall B. Blood and tissue spatter associated with a chainsaw dismemberment. J Forensic Sci 2009;54(6):1310–4.
8. Sweet MJ. Velocity measurements of projected bloodstains from a medium velocity impact source. Can Soc Forensic Sci J 1993;26(3):103–10.
9. Pizzola PA, Roth S, De Forest PR. Blood droplet dynamics—I. J Forensic Sci 1986;31(1):36–49.
10. Hulse-Smith L, Mehdizadeh NZ, Chandra S. Deducing drop size and impact velocity from circular bloodstains. J Forensic Sci 2005;50(1):54–63.
11. Knock C, Davison M. Predicting the position of the source of blood stains for angled impacts. J Forensic Sci 2007;52(5):1–6.
12. Laber TL, Epstein BP, Taylor MJ. High speed digital video analysis of bloodstain pattern formation from common bloodletting mechanisms. IABPA News: June 2008:4–12.
13. Rein M. Phenomena of liquid drop impact on solid and liquid surfaces. Fluid Dyn Res 1993;12:61–93.
14. Gelfand BM. Droplet breakup phenomena in flows with velocity lag. Prog Energy Combust Sci 1996;22:201–65.
15. Lin SP. Drop and spray formation from a liquid jet. Annu Rev Fluid Mech 1998;30:85–105.
16. Wells JK. Investigation of factors affecting the region of origin estimates in bloodstain pattern analysis [Master's Thesis]. Canterbury (New Zealand): University of Canterbury, 2006.

Additional information and reprint requests:
Lee Hulse-Smith, M.Sc.
Centre of Forensic Sciences
Biology Section, 4th Floor
25 Grosvenor Street
Toronto, ON M7A 2G8
Canada
E-mail: lee.hulsesmith@ontario.ca